Orthopaedic Surgery

RESEARCH ARTICLE OPEN ACCESS

Biomechanical Comparison of a Novel Facet Joint Fusion Fixation Device With Conventional Pedicle Screw Fixation Device: A Finite Element Analysis

Feilong Sun | Haiyang Qiu | Yufei Ji | Longchao Wang | Wei Lei | Yang Zhang

Department of Orthopedics, Xijing Hospital, Air Force Medical University, China

Correspondence: Yang Zhang (zhangyang@fmmu.edu.cn)

Received: 23 September 2024 | **Revised:** 21 January 2025 | **Accepted:** 9 February 2025

Funding: This research was supported by the Key Research and Development Program of Shaanxi Province of China (2023-YBSF-146).

Keywords: biomechanical study | facet joint | finite element analysis | lumbar spine | pedicle screw

ABSTRACT

Purpose: The biomechanics of a novel facet joint fusion device is unknown. The objective of this study is to analyze and compare the biomechanical properties of a novel facet joint fusion device integrated with oblique lateral interbody fusion (OLIF) to those of a conventional pedicle screw fixation device, employing finite element analysis.

Methods: A comprehensive three-dimensional finite element model of the L3-S1 lumbar spine was developed and validated. Based on this model, three surgical groups were created: OLIF combined with the bilateral facet joint fusion fixation (BFJFF + OLIF), unilateral pedicle screw fixation (UPSF + OLIF), and bilateral pedicle screw fixation (BPSF + OLIF), focusing on the L4-L5 level. A torque of 7.5 Nm was applied to simulate vertebral activities under six conditions: flexion, extension, lateral bending (left and right), and axial rotation (left and right). The maximum displacement at the L4-L5 segment was then calculated. The maximum stress values were recorded at the L4-L5 interbody fusion cage and the L3-L4 and L5-S1 segments.

Results: When compared to the other two models, the BFJFF + OLIF model exhibited the smallest maximum displacement value at the L4-L5 segment across all six working conditions. The BFJFF + OLIF model also demonstrated the lowest maximum stress value at the L4-L5 segment interbody fusion cage under flexion, as well as left and right lateral bending and axial rotation conditions when compared with the other models. However, under the extension condition at the L4-L5 interbody fusion cage, the BPSF + OLIF model showed the lowest maximum stress value. At the adjacent L3-L4 segments, the BFJFF + OLIF model registered the lowest maximum stress value during flexion and left lateral bending conditions. At L3-L4, under extension and right lateral bending conditions, the UPSF + OLIF model exhibited the lowest maximum stress value. Under left axial rotation at the L3-L4 segment, both the BFJFF + OLIF and UPSF+OLIF models demonstrated the smallest maximum stress values. Under right axial rotation at the L3-L4 segment, the BPSF + OLIF model recorded the smallest maximum stress value. Concurrently, at the L5-S1 segment, the BFJFF + OLIF model presented the lowest maximum stress value under conditions of flexion, as well as left and right lateral bending and axial rotation. In the L5-S1 segment during the extension condition, the UPSF+OLIF model exhibited the lowest maximum stress value.

Conclusions: This study demonstrates that the novel device, when combined with OLIF, achieves 360° lumbar fusion by fusing the lumbar facet joints, thereby enhancing spinal stability post-fusion. Concurrently, stress on adjacent segments was diminished.

Feilong Sun, Haiyang Qiu and Yufei Ji contributed equally to this study.

The findings suggest that this device may serve as a novel internal fixation method. It may provide a new option for the surgical treatment of patients with low back pain in the future.

1 | Introduction

Facet Joint Osteoarthritis (FJOA) is characterized by degenerative changes in the synovium, articular cartilage, subchondral bone, joint space, and accessory tissues of the spinal facet joints, influenced by various factors [1]. Imaging studies show that more than 70% of adults aged 60 and older display signs of FJOA [2]. Patients often exhibit a range of symptoms, including local pain and movement disorders. Without intervention, disease progression can lead to severe facet joint hyperplasia and reduced biomechanical integrity, resulting in intervertebral instability, spondylolisthesis, and spinal stenosis, which significantly impairs patient quality of life. In the early stages of FJOA, treatment primarily involves conservative approaches such as local immobilization, physiotherapy, pharmacological interventions, and nerve blocks. For advanced FJOA, surgical intervention often becomes necessary, with lumbar interbody fusion being a common approach. Given the limitations of existing treatments, this study presents a novel spinal facet joint fusion fixation (FJFF) device, designed to facilitate comprehensive fusion of the spine's three-joint complex alongside interbody fusion. This innovative device not only improves spinal stability but also maintains range of motion (ROM) and slows the degeneration of adjacent spinal segments.

Common lumbar interbody fusion techniques encompass anterior lumbar interbody fusion (ALIF), posterior lumbar interbody fusion (PLIF), transforaminal lumbar interbody fusion (TLIF), and oblique lateral interbody fusion (OLIF) [3]. OLIF, a minimally invasive surgical technique, provides advantages including reduced operation time, minimal intraoperative blood loss, and shorter hospital stays [4]. Reports suggest that OLIF alone can result in complications such as cage displacement, frequently necessitating combination with posterior percutaneous pedicle screw fixation [5, 6]. Inadequate interbody fusion may cause posterior screw displacement, resulting in complications like spondylolisthesis. Considering the new device's capability to fuse facet joints, its combination with OLIF to achieve 360° vertebral body fusion using a minimally invasive approach was proposed. Consequently, finite element analysis was used to assess the biomechanics of the new facet joint fusion device combined with OLIF, aiming to replace pedicle screw fixation, achieve equivalent fusion effects, and evaluate impacts on adjacent segments. Originating in the 1950s, finite element analysis has become a staple in orthopedic engineering. This method facilitates constructing mathematical models tailored to specific experimental needs, allowing for the study of stress on spinal implants under various loads, interactions between implants and bones, and biomechanical comparisons among different implants [7, 8]. Liu et al. used finite element analysis to investigate the biomechanics of OLIF combined with various fixation devices in osteoporotic patients [9]. Cai et al.'s study indicated that combining OLIF with bilateral pedicle screw fixation could optimally maintain spinal stability [10]. To determine the long-term biomechanical effects of the new facet joint fusion device on the lumbar spine, a three-dimensional (3D) finite element model was developed. Three models were created: OLIF with bilateral facet joint fusion fixation (BFJFF + OLIF), unilateral pedicle screw fixation (UPSF + OLIF), and bilateral pedicle screw fixation (BPSF + OLIF). The purpose of this study was to investigate the three models using finite element analysis to investigate (i) the stability of the L4-L5 segment, (ii) the stress of the interbody fusion cage at the L4-L5 segment, and (iii) the stress of the adjacent segments. Finite element analysis enabled the comparison of biomechanical differences among the models, offering insights for future clinical applications.

2 | Materials and Methods

2.1 | Design and Construction of the Device

The novel FJFF device proposed in this study comprises a gasket component and a screw fixation component. The anterior spacer and posterior screw fixation components are integrated. The screw fixation component features two screw holes for secure attachment, while the gasket component includes a bone grafting groove and an anti-exit barb. The novel FJFF device has been patented in China under patent number ZL20232 2333005.3. The new one-piece device can be manufactured via 3D printing with Ti6Al4V powder. The integration of the front shim and posterior screw fixation components enables the implantation of two screws into the posterior section, securing the device to the bone. Simultaneously, autogenous bone was packed into the graft groove of the anterior spacer, facilitating bone growth with the upper and lower articular surfaces to achieve fusion and fixation of the device with the bone. The gasket component is positioned within the surgical facet joint space, with the screw fixation component affixed to the corresponding upper and lower facet joints. The detailed operational procedure is illustrated in Figure 1.

2.2 | Modeling of the Normal Lumbar Spine

Modeling Process: A comprehensive geometric model of the lumbar spine was constructed using Mimics19.0 software (Materialise, Leuven, Belgium), based on computed tomography images of the T1 vertebra and below from a healthy 25-year-old male volunteer. Subsequently, the surface was generated using Geomagic Studio 2013 (Geomagic Inc., North Carolina, USA), and the model was meshed and its material properties assigned using HyperMesh14.0 (Altair Engineering ROMCorp., Michigan, USA). The model's contact settings and load parameters were then defined using Abaqus6.12 (Dassault Systemes Simulia Corporation, Pennsylvania, USA), followed by the execution of the analysis. Material and cross-sectional properties were defined based on established parameters for cortical bone, cancellous bone, cartilage endplates, spinous processes, annulus fibrosus, and nucleus pulposus as documented in prior literature. Interactions between cortical and cancellous bone, implants and bone, and intervertebral discs and bone

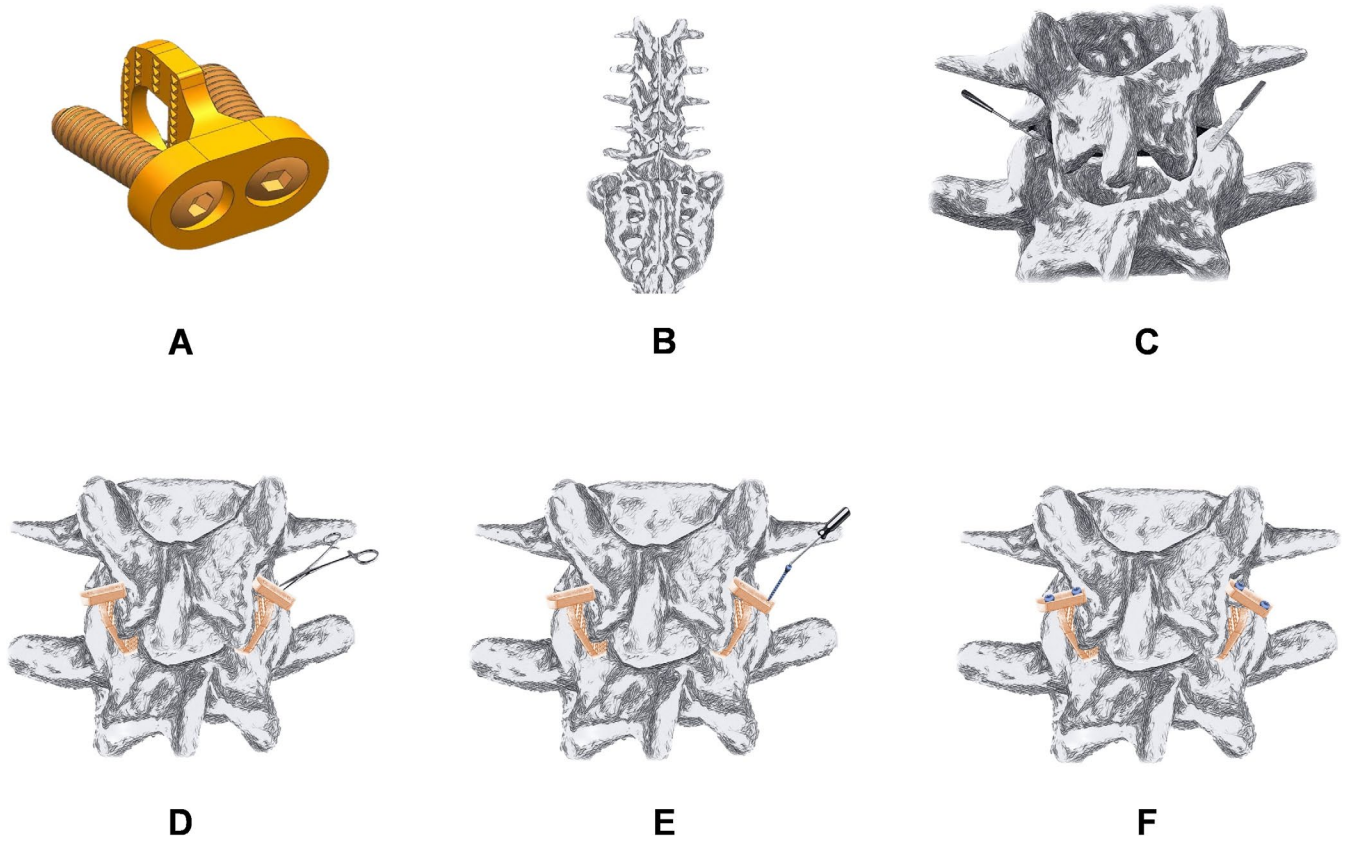

FIGURE 1 | Schematic diagram of the novel facet joint fusion fixation (FJFF) device and surgical procedure. (A) Schematic of the novel device; (B) the L4-L5 segment was identified as the surgical target; (C) the articular surface of the facet joint at the L4-L5 level was treated with a curette, and a bone fusion bed was prepared by bone rubbing; (D) the new device was positioned and inserted along the prepared trajectory of the L4-L5 facet joint space; (E) the device was secured by screwing into the superior and inferior facet joint bones of the adjacent vertebral body; (F) diagram of the new device successfully installed.

were classified as "binding," while the interface between articular cartilage and bone was designated as "contact." The coefficient of friction was set at 0.2. Material properties for major ligaments—including the anterior and posterior longitudinal, supraspinous, interspinous, ligamentum flavum, joint capsule, and intertransverse ligaments—were defined based on previous literature (Table 1) [11–14]. The established finite element model is depicted in Figure 2.

2.3 | Modeling of Lumbar Spine Surgery

This study established three lumbar surgery models (Figure 3): BPSF + OLIF, BFJFF + OLIF, and UPSF + OLIF. Research has demonstrated that FJOA frequently occurs in the L4-L5 segments [15]. Consequently, the L4-L5 segment has been selected as the focus for surgical interventions in this study.

Using Unigraphics NX10.0 Software (Siemens PLM Software Corporation, Texas, USA), the entire nucleus pulposus and part of the annulus fibrosus were removed to simulate the partial disc removal characteristic of the OLIF procedure. Subsequently, the OLIF cage and all fixation instruments were modeled. The positions of these components were then adjusted to align with the model, followed by the assembly of each group of models. Different fixation devices were incorporated into the L4-S5 segments, as depicted in Figure 4.

Figure 5 displays schematics of the fixtures. The central point of the screw served as the measurement reference. The pedicle screw measures 45 mm in length and 6.5 mm in diameter. The connecting rod has a diameter of 6 mm; the new facet joint fusion device features a thickness of 2 mm, with screws measuring 13 mm in length and 4 mm in diameter. The disc cage measures 45 mm in length, 22 mm in width, 9.5 mm in height, and has a surface area of 28.21 cm^2. The intermediate bone graft consists of cancellous bone, with the screw-rod, screw-bone, and cage-endplate interactions designated as "binding" relationships. Material characteristics are detailed in Table 1. The complete model is depicted in Figure 2, and the surgical model is shown in Figure 3.

2.4 | Loading and Boundary Conditions

In this study, the sacrum was immobilized with the boundary conditions specifying that the middle and posterior structures of the sacrum were fixed without displacement or rotation. Typically, the lumbar spine supports significant compressive loads from the upper body weight, playing a crucial role in maintaining spinal stability and enhancing load-bearing capacity. Consequently, a coupling point was established at the center of the upper endplate of L3, where a vertical downward force of 500 N was applied to simulate the upper body load on the lumbar spine under normal conditions [16]. Additionally,

TABLE 1 | Material assignments for the normal lumbar spine FEA model and the surgical model.

Components	Young's modulus (MPa)	Poisson's ratio	Type element	Cross-sectional area (mm^2)
Cortical bone	12,000	0.3	C3D4	
Cancellous bone	100	0.3	C3D4	
Nucleus pulposus	1	0.499	C3D4	
Annulus fibrosus	4.2	0.45	C3D4	
Facet cartilage	25	0.4	C3D4	
Cartilage endplate	24	0.4	C3D4	
Screw and rods	110,000	0.3	C3D4	
Cage	110,000	0.3	C3D4	
Anterior longitudinal ligaments	28	0.45	T3D2	38
Posterior longitudinal ligaments	24	0.45	T3D2	20
Ligamentum flavum	7	0.45	T3D2	60
Intertransverse ligament	10	0.45	T3D2	36
Capsular Ligament	7.5	0.45	T3D2	30
Interspinous ligament	10	0.45	T3D2	35.5
Supraspinous ligament	8	0.45	T3D2	35.5

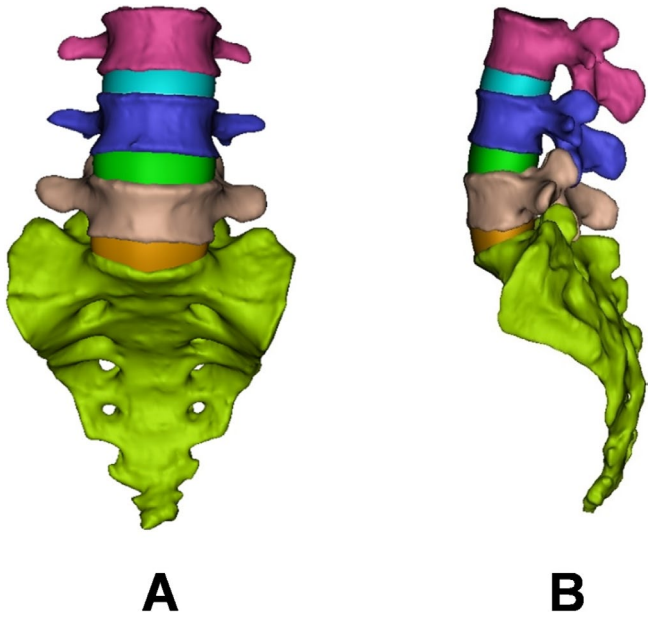

FIGURE 2 | FEA model of normal lumbar spine (L3-S1). (A) Frontal position; (B) lateral position.

a torque of 7.5 Nm was applied to the upper endplate of L3, permitting movement within the physiological range without damaging the tissue structure [17]. A compressive preload was applied to the finite element model of the normal lumbar spine (L3-S1) shown in Figure 2, and to the various surgical fixation models depicted in Figure 3. Based on these constraints and loading conditions, relevant data were imported into Abaqus6.12 for analysis to simulate the lumbar spine's ROM in flexion, extension, lateral bending (left and right), and axial rotation (left and right) under six working conditions. Displacement and stress distribution at L4-L5 and adjacent segments were recorded for each model under vertical physiological loading.

2.5 | Data Collection and Model Validation

This study generated displacement cloud maps of the L4-L5 segment of the finite element model (L3-S1) using various fixation devices. Equivalent stress values for the cage and intervertebral discs at adjacent segments (L3-L4, L5-S1) were calculated. Von Mises stress, a yield criterion, is commonly quantified as the equivalent stress value. It describes the internal stress distribution within the model, highlighting areas under maximum stress for rapid identification and necessary adjustments. ROM refers to the mobility between adjacent lumbar spine segments. Subsequently, Abaqus finite element analysis software was used to compute and export these values for further analysis. The comprehensive L3-S1 model was compared with existing literature to validate its accuracy [18, 19].

3 | Results

3.1 | Validation of the Finite Element Model

The complete L3-S1 finite element model comprised cortical bone, cancellous bone, nucleus pulposus, annulus fibrosus, and ligaments. The materials used are detailed in Table 1. A pure moment of 7.5 Nm was applied to the L3 vertebral body in the complete L3-S1 model to determine the ROM for the L4-L5 segments during flexion, extension, lateral bending

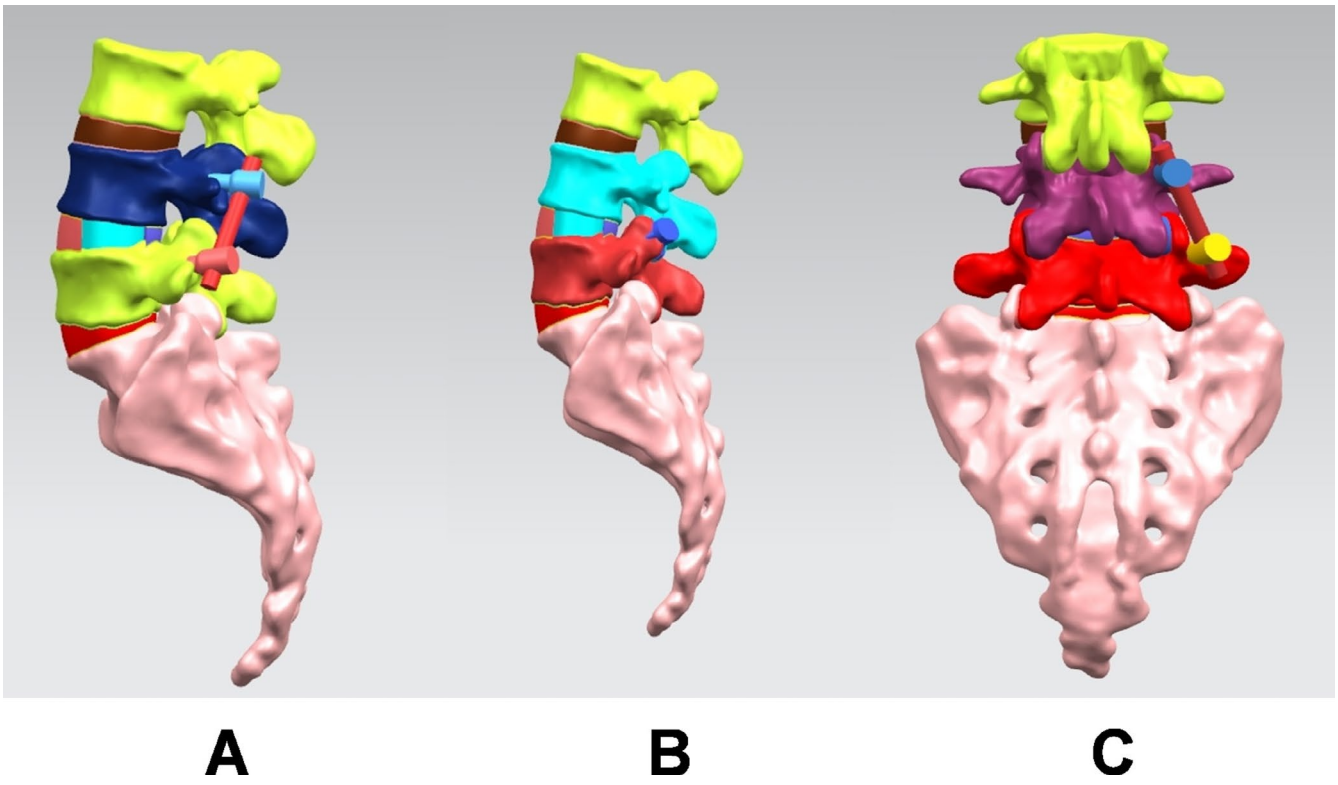

FIGURE 3 | FEA model of the operated lumbar spine (L3-S1). (A) BPSF + OLIF; (B) BFJFF + OLIF; (c) UPSF + OLIF.

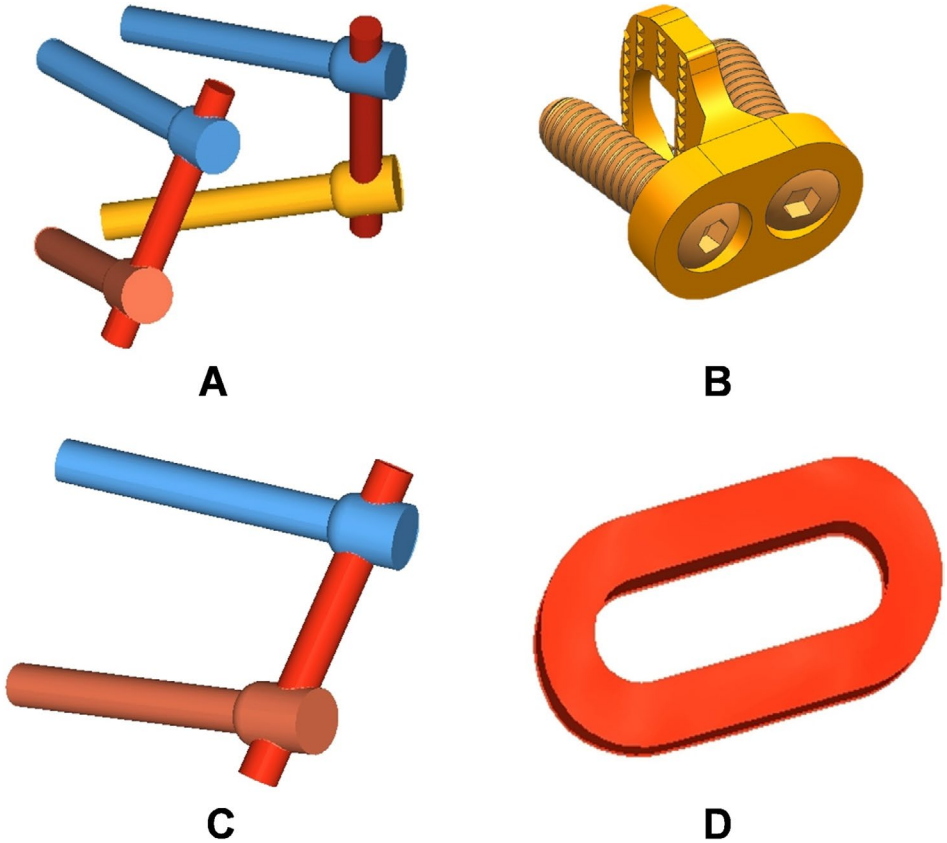

FIGURE 4 | (A) Bilateral pedicle screws; (B) new facet joint fusion fixation device; (C) unilateral pedicle screws; (D) intervertebral disc fusion device.

(left and right), and axial rotation (left and right). This range was comparable to measurements reported by Vadapalli et al. and Yang et al. (Figure 6). This outcome indicates that the model accurately simulates the actual motion of the lumbar spine. Furthermore, this model can be used to analyze biomechanical changes in the lumbar spine under various loads [18, 19].

3.2 | Maximum Displacement Analysis of Various Modeled L4-L5 Segments at Six Operating Conditions

Figure 7 displays the maximum displacement values for each model group at the L4-L5 level. Under flexion, the BPSF + OLIF, BFJFF + OLIF, and UPSF + OLIF models exhibited maximum displacements of 4.17, 2.96, and 3.59 mm, respectively. Under extension, the three models displayed maximum displacements of 0.47, 0.35, and 0.60 mm, respectively. During left lateral bending, the models recorded maximum displacements of 2.36, 1.67, and 1.93 mm, respectively. In right lateral bending, the models achieved maximum displacements of 1.84, 1.54, and 1.90 mm, respectively. Under left axial rotation, the maximum displacements were 1.90, 1.58, and 1.86 mm for the models, respectively. For right axial rotation, the models demonstrated maximum displacements of 1.85, 1.52, and 1.83 mm, respectively. As illustrated in Figure 7, the BFJFF + OLIF model exhibits smaller displacements than the other two models at the L4-L5 segments under six conditions: flexion, extension, left and right lateral flexion, and left and right axial rotation.

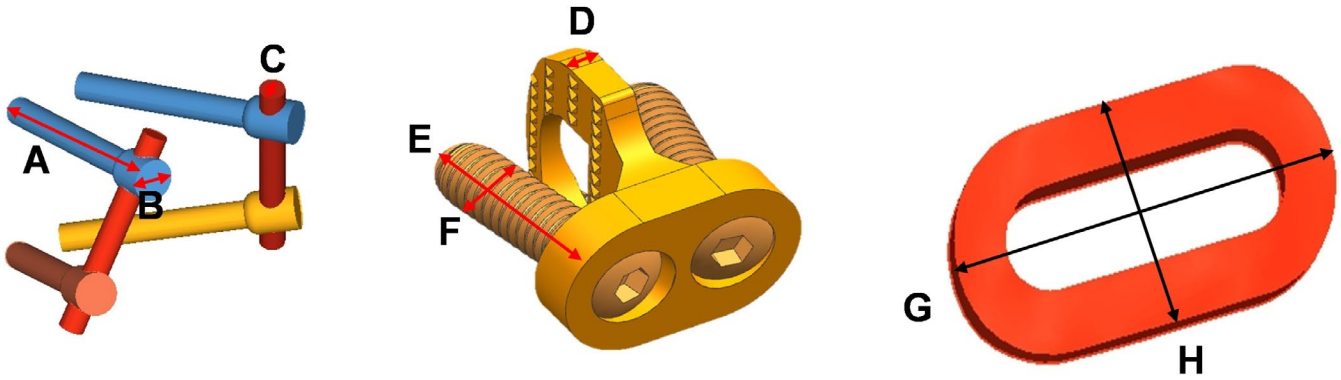

FIGURE 5 | Diagram of the position of the fixation device. (A) Pedicle screw length; (B) diameter of pedicle screws; (C) diameter of the connecting rod; (D) thickness of the new facet joint fusion fixation device spacer; (E) length of the new facet joint fusion fixation device screw; (F) diameter of the new facet joint fusion fixation device screws; (G) interbody fusion length; (H) interbody fusion device width.

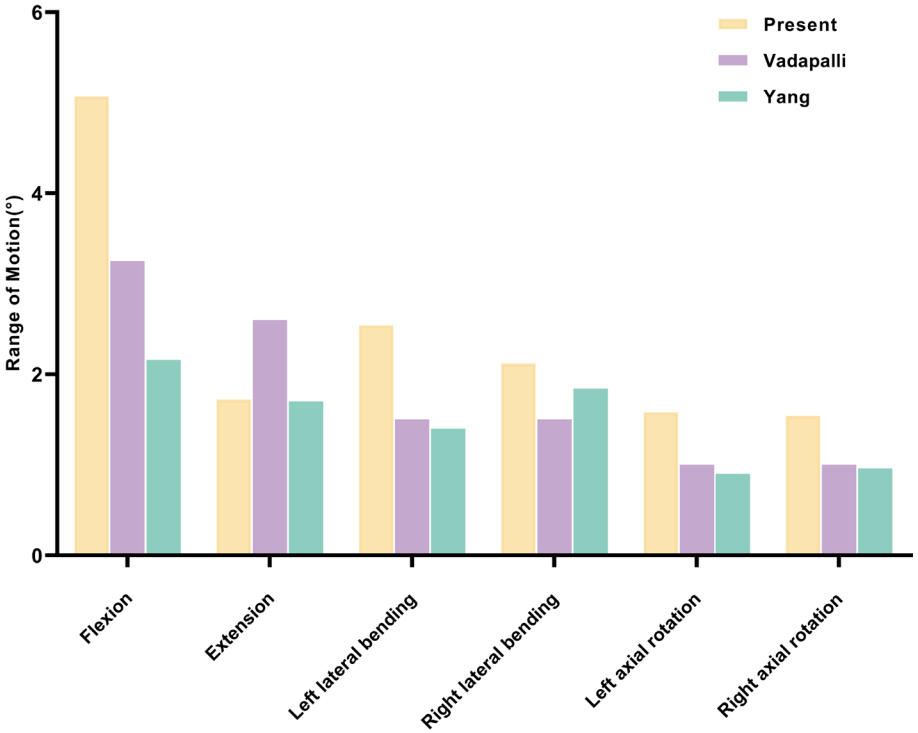

FIGURE 6 | The ROM for the L4-L5 segment in the complete model was validated and compared with previous studies under conditions of flexion, extension, left and right lateral flexion, and left and right axial rotation.

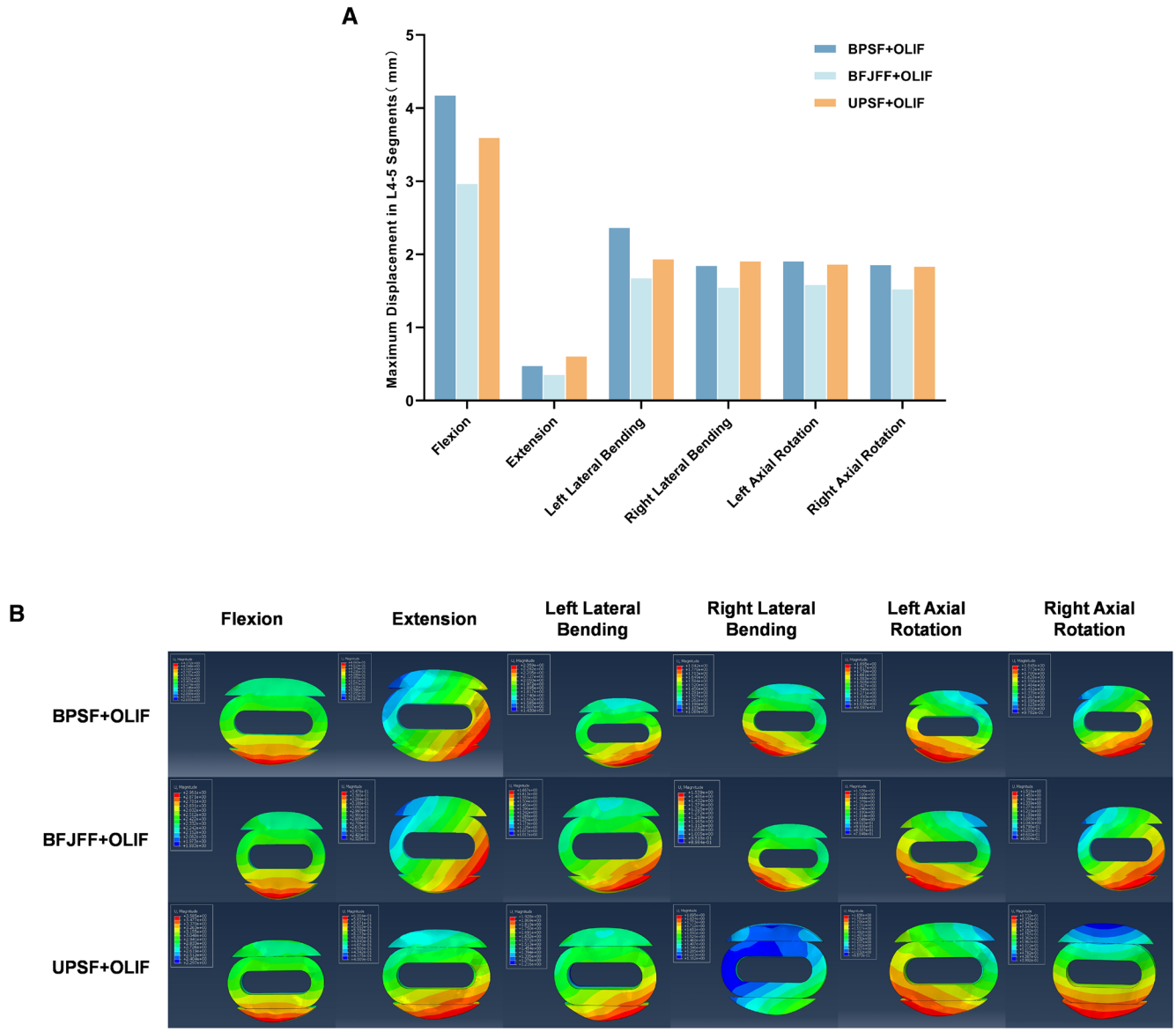

FIGURE 7 | Maximum displacement values (A) and displacement cloud diagram (B) for three different lumbar fusion models (L4-L5).

3.3 | Maximum Stress Analysis of the OLIF Fusion Cage at the L4-L5 Segment of Various Models Under Six Operating Conditions

Figure 8 displays stress maps for the interbody fusion cages at the L4-L5 level across various models. Under flexion, the OLIF cages at the L4-L5 segment exhibited maximum stresses of 9.63, 7.93, and 9.58 MPa in the BPSF + OLIF, BFJFF + OLIF, and UPSF + OLIF models, respectively. During extension, the OLIF fusion cages at the L4-L5 segment recorded maximum stresses of 3.41, 4.12, and 7.45 MPa for the three model groups, respectively. In left lateral bending, the OLIF fusion cages at the L4-L5 segment showed maximum stresses of 8.80, 6.18, and 8.48 MPa in the three models, respectively. Under right lateral bending, the maximum stresses for the OLIF fusion cages at the L4-L5 segment were 8.26, 5.96, and 7.67 MPa for each model group, respectively. During left axial rotation, the OLIF fusion cages at the L4-L5 segment experienced maximum stresses of 6.05, 4.87, and 6.28 MPa in the three models, respectively. In right axial rotation, the OLIF fusion cages at the L4-L5 segment registered maximum stresses of 6.33, 4.52, and 5.01 MPa for each respective model group. As shown in Figure 8, the BFJFF + OLIF model demonstrates the lowest stress at the L4-L5 segment under flexion, left and right lateral bending, and left and right axial rotation. In the extension condition, the BFJFF + OLIF model exhibited higher stress at the L4-L5 segment than the BPSF + OLIF model but lower than the UPSF + OLIF model.

3.4 | Maximum Stress Analysis of Neighboring Segments (L3-L4, L5-S1) of Various Models at Six Working Conditions

Figures 9 and 10 display the stress analysis for each model at the L3-L4 and L5-S1 segments, respectively. Figure 9 shows that under flexion, the L3-L4 segment of the BPSF + OLIF, BFJFF + OLIF, and UPSF + OLIF models registered maximum stress values of 0.97, 0.87, and 0.95 MPa, respectively. In the

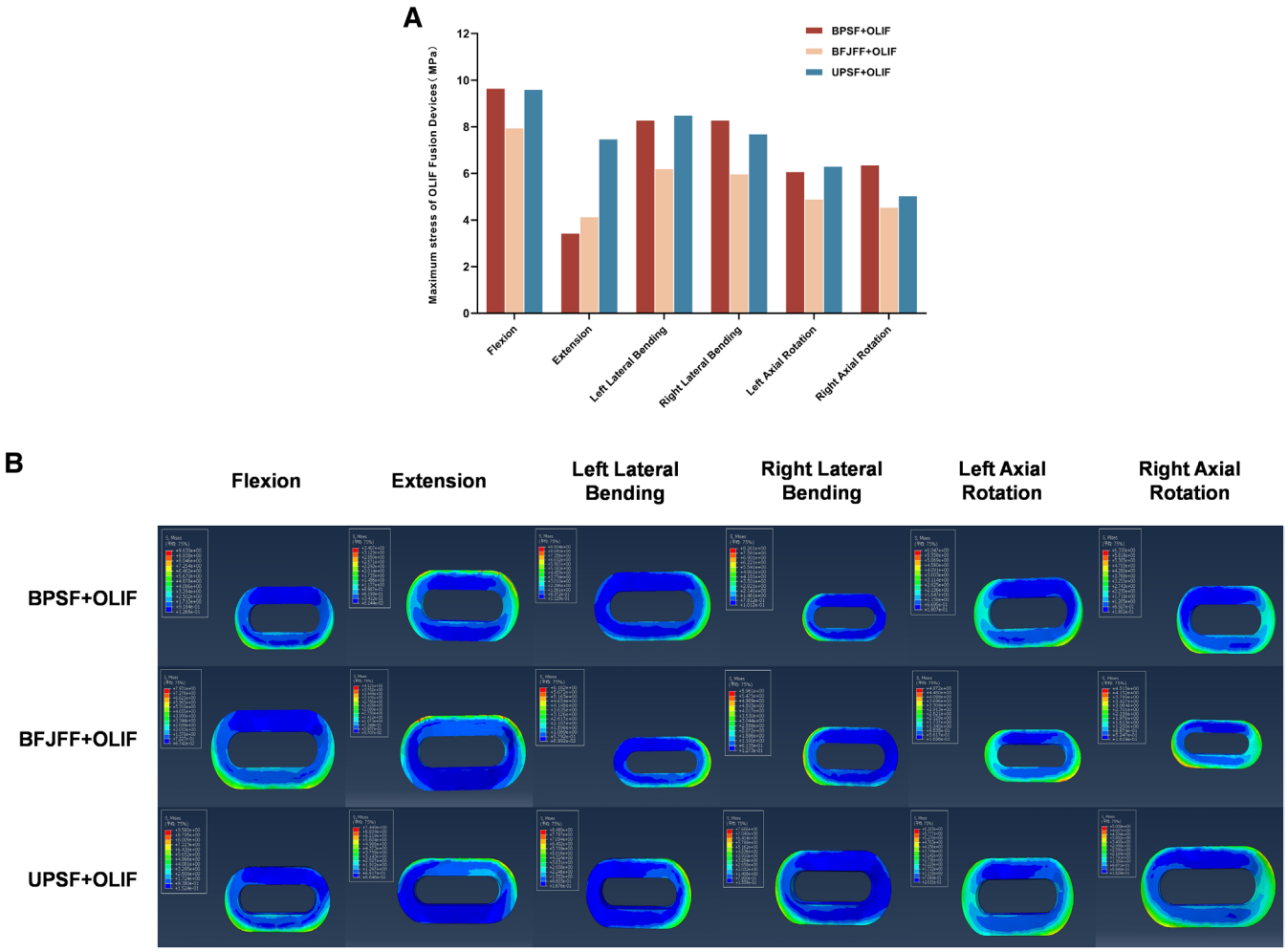

FIGURE 8 | Maximum stress values (A) and stress cloud diagram (B) of L4-L5 interbody fusion cage in three lumbar fusion models under different working condition Figure 8. Maximum stress values (A) and stress cloud diagram (B) of L4-L5 interbody fusion cage in three lumbar fusion models under different working conditions.

extension condition, the L3-L4 segment experienced maximum stresses of 1.04, 1.04, and 0.99 MPa in the three models, respectively. During left lateral bending, the L3-L4 segment showed maximum stresses of 1.10, 0.97, and 1.09 MPa for each model group, respectively. Under right lateral bending, maximum stresses at the L3-L4 segment were 1.10, 0.95, and 0.94 MPa for the respective models. In left axial rotation, the L3-L4 segment had maximum stresses of 0.75, 0.70, and 0.70 MPa for the respective model groups. During right axial rotation, the maximum stresses at the L3-L4 segment were 0.67, 0.69, and 0.70 MPa for the three models, respectively. It is evident that under flexion, left lateral bending, and left axial rotation, the BFJFF + OLIF model exhibits lower stress values in the L3-L4 segment, which are comparable to those of the UPSF + OLIF model under extension. Under right lateral bending, the stress value of the BFJFF + OLIF model in the L3-L4 segment was lower than that of the BPSF + OLIF model and slightly higher than that of the UPSF + OLIF model. However, the stress value of the BFJFF + OLIF model in the L3-L4 segment under right axial rotation condition was completely opposite to that under right lateral bending condition.

Figure 10 illustrates that under flexion, the maximum stress values at the L5-S1 segment for the BPSF + OLIF, BFJFF + OLIF, and UPSF + OLIF models were 1.29, 1.06, and 1.25 MPa, respectively. In the extension condition, the L5-S1 segment experienced maximum stresses of 0.62, 0.41, and 0.38 MPa in the three models, respectively. In the left lateral bending condition, the L5-S1 segment's maximum stresses for the three model groups were 1.47, 0.96, and 1.16 MPa, respectively. During right lateral bending, the maximum stress values at the L5-S1 segment were 1.08, 0.83, and 0.87 MPa for each group, respectively. Under left axial rotation, the maximum stress values at the L5-S1 segment for the three models were 1.10, 0.88, and 1.02 MPa, respectively. Under the right axial rotation condition, the L5-S1 segment's maximum stress values were 0.95, 0.75, and 0.83 MPa for the three models, respectively. The maximum stress values of the BFJFF + OLIF model at the L5-S1 segment were lower than those of the other two models under conditions of flexion, left and right lateral bending, and left and right axial rotation. Under extension, the maximum stress value of the BFJFF + OLIF model at the L5-S1 segment was lower than that of the BPSF + OLIF model but slightly higher than that of the UPSF+OLIF model.

4 | Discussion

This study established finite element models for three advanced FJOA surgical techniques. Relevant biomechanical parameters,

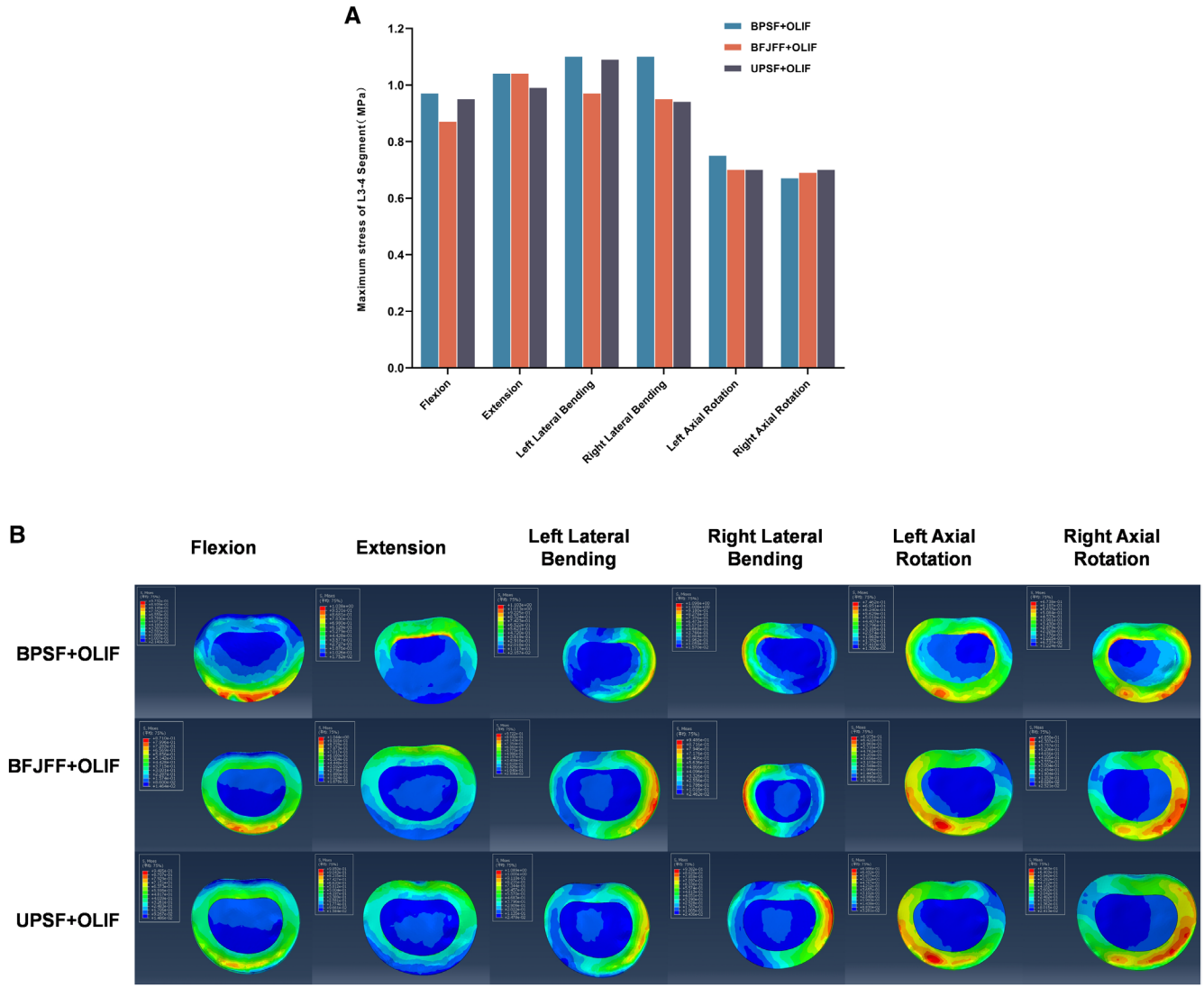

FIGURE 9 | Maximum stress values (A) and stress cloud diagram (B) at L3-L4 of three lumbar fusion models under various working conditions.

including L4-L5 displacement, OLIF cage stress at the L4-L5 level, and stresses at the L3-L4 and L5-S1 levels, were analyzed to determine biomechanical variations across different instruments and their impact on spinal stability and load distribution [5, 20–22]. A finite element model of the intact L3-S1 lumbar spine was developed and validated against similar models cited in the literature [18, 19]. Consequently, the developed finite element model facilitates comparisons of lumbar spine mobility and stress distribution among various fixation devices.

4.1 | Structural Differences From Other Facet Joint Fixators

In 2006, Goel et al. introduced a novel treatment for lumbar degenerative diseases involving the insertion of devices into the lumbar facet joints. He conducted facet joint fusion on 21 patients with lumbar spinal stenosis by implanting circular devices with bone graft grooves into the lumbar facet joints. All patients experienced positive therapeutic outcomes without any implant displacement. The insertion of spacers restored the height of the facet joints and maintained spinal segment stability [23, 24]. Further research on human lumbar spine specimens indicated that spacer insertion in facet joints increased the height of intervertebral discs and vertebral bodies, confirming its viability for treating conditions like spinal stenosis [25]. Srour et al. conducted facet arthrodesis using a D-shaped spacer in 53 patients with lumbar spinal stenosis and facet joint syndrome; while one patient experienced implant displacement post-surgery, all reported symptom improvement [26]. Simultaneously, Srour compared D-shaped facet joint fusion devices with pedicle screw fixation, noting significant reductions in intraoperative blood loss and surgical time, although one patient experienced implant displacement [27]. Simon et al. utilized finite-element analysis to compare D-pads with pedicle screws, discovering that the facet joint fusion device alleviated stress on adjacent segments, thus delaying their degeneration [7]. This study proposes a new FJFF device comprising a shim part and a screw fixation part. This device not only fuses the facet joint via the shim but also secures it with screws, minimizing internal displacement and delaying adjacent segment degeneration.

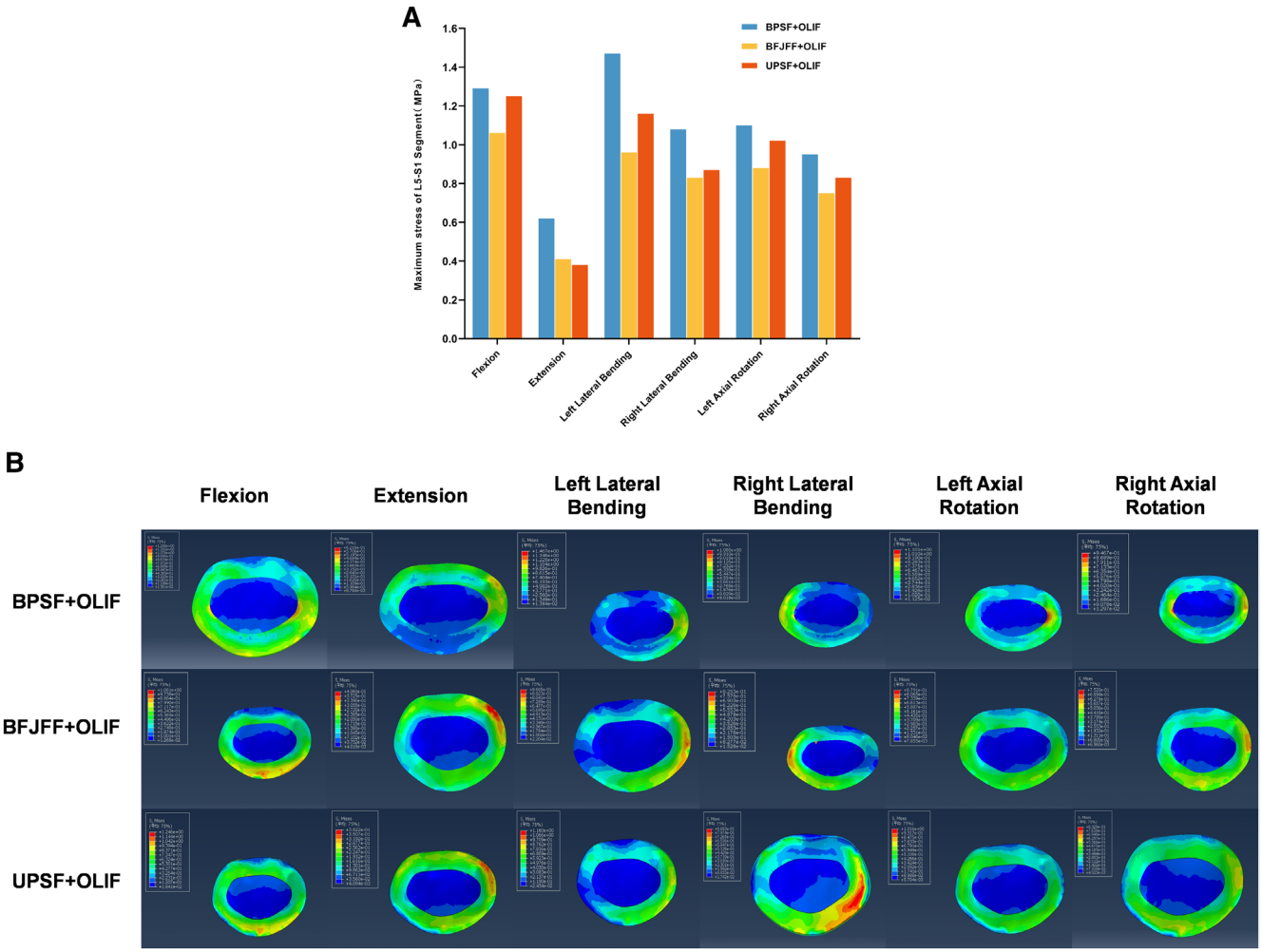

FIGURE 10 | Maximum stress values (A) and stress cloud diagram (B) at L5-S1 of three lumbar fusion models under various working conditions.

4.2 | Biomechanical Effects of OLIF Combined With Various Internal Fixation Devices

OLIF offers several advantages over other interbody fusion procedures, including smaller incisions, reduced blood loss, shorter hospital stays, and quicker recovery. In recent years, OLIF has become widely utilized in clinical practice [28–30]. However, OLIF surgery alone may lead to postoperative complications, including cage displacement, subsidence, and nonfusion [6, 31]. Fang et al. demonstrated that bilateral pedicle screw fixation significantly reduces the incidence of cage subsidence during OLIF compared to OLIF alone [5]. Pan et al. found that stress values of the OLIF cage are lower in the bilateral pedicle screw fixation model compared to the unilateral model, a conclusion also supported by our study [20]. This reduction in stress may be attributed to the use of two pedicle screws in OLIF surgery, which enhance the external protection of the surgical segment, thereby diminishing the deformation force on the interbody fusion cage during vertebral movement.

4.3 | Stability Effect of the Surgical Segments

Surgical segment stability is a crucial success indicator, as instability can result in complications like spondylolisthesis, spinal stenosis, and cage nonfusion, all of which may cause pain and deteriorate the patient's quality of life [6, 26, 32]. Our findings indicate that the new device exhibited the smallest displacement values under all six conditions when compared to both unilateral and bilateral pedicle screw fixation (Figure 7). This enhanced stability may stem from the new device's integration of facet joint fusion with interbody fusion cage fixation, effectively fusing the three-joint complex and substantially increasing vertebral stability. The reduced deformation force partially reflects the improved stability offered by the new device, which increases the surgical segment's stiffness to varying degrees, illustrating the varied impact of different fixation devices on segment stability. Increased stiffness of the operated segment correlates with enhanced segment stability. Pan et al. found that bilateral pedicle screw fixation offers superior vertebral stability compared to unilateral fixation [20]. Cai et al. demonstrated that bilateral pedicle screw fixation in OLIF surgery enhances lumbar stability, resists cage subsidence, and preserves disc height [11]. The results indicate that the new device achieves greater vertebral stability than bilateral pedicle screw fixation in OLIF surgery.

4.4 | Biomechanical Effects on Adjacent Segments

Adjacent segment degeneration describes the degenerative changes in segments adjacent to a lumbar fusion site. This

condition not only impacts the long-term effectiveness of lumbar fusion but also increases the likelihood of reoperation, which typically has a lower success rate than the initial surgery [33–35]. While the precise mechanisms underlying adjacent segment degeneration remain unclear, it is hypothesized that interbody fusion can increase pressure on adjacent segments [36]. Weinhoffer et al. found that pressure in adjacent segments was higher in the fused group than in the unfused group at the same flexion angle [37]. Cunningham et al. reported increased motion and pressure in adjacent unfused segments following fusion [38]. To mitigate the degeneration of adjacent segments, Rana et al. modified the structure of the pedicle screw connecting rod to decrease stress concentration and segment rigidity, thereby reducing stress on adjacent segments and delaying their degeneration [39, 40]. Concurrently, Kim et al. demonstrated that, compared to traditional rigid rods, using semi-rigid rods with pedicle screws increases the ROM in the surgical segment and decreases it in adjacent segments, thus minimizing compensatory stress and benefiting the delay of adjacent segment degeneration [41]. Increasing pressure on the adjacent intervertebral disc segment leads to disc deformation. This deformation, in turn, reduces the disc's height and alters its properties, ultimately diminishing the disc's ability to deform and reducing its ROM. In this study, at the L3-L4 segment (Figure 9), the BFJFF + OLIF model exhibited lower stress compared to the other two models under flexion, left lateral bending, and left axial rotation conditions. For the L5-S1 segment (Figure 10), the stress in the BFJFF + OLIF model was slightly higher than in the UPSF + OLIF model under specific working conditions, yet it was lower than the other two models in all other conditions. The findings indicate that the new device can reduce stress on adjacent segments, thereby potentially delaying their degeneration.

4.5 | Strengths and Limitations

This study introduces a novel lumbar FJFF device and investigates its biomechanical differences from traditional pedicle screw fixation when combined with OLIF, using finite element analysis. The findings indicate that combining the new device with the OLIF procedure enhances stability at the surgical site and reduces stress on adjacent segments. This suggests its viability as an alternative for patients with advanced FJOA requiring interbody fusion following unsuccessful conservative treatments. Concurrently, this experiment represents the first application of finite element analysis to this new device. Following targeted improvements based on these results, the device's efficacy was further validated through subsequent in vitro human specimen tests and in vivo animal studies.

However, this study has several limitations. The study did not account for the effects of paravertebral muscles and motion on loading, which could influence the actual motion and stress distribution of the lumbar spine. Secondly, the complex 3D structure of ligaments was difficult to replicate accurately, necessitating simplification. Additionally, the motion load was set at 7.5 Nm across all working conditions, without comparing how different loads might affect the models. Similar to other finite element analysis studies and biomechanical tests, this experimental model aimed to elucidate the biomechanical effects of various surgical procedures on the spine, allowing for the measurement and comparison of data across procedures to foster further advancements.

4.6 | Prospect of Clinical Application

This study demonstrated that the novel FJFF device impacts spinal biomechanics differently than pedicle screw fixation. The novel FJFF device consists of an anterior gasket component and a posterior screw fixation section, into which two screws can be implanted to secure the device to the bone. Simultaneously, autogenous bone was packed into the graft groove of the anterior spacer, facilitating growth with the upper and lower articular surfaces and achieving fusion and stabilization of the device with the bone. The FJFF device enhances vertebral stability and ROM, achieving fusion of the three-joint complex via facet joint fusion and thereby reducing postoperative complications such as spondylolisthesis and spinal stenosis. Furthermore, the FJFF device reduces stress on adjacent segments, minimizing their impact to the greatest extent possible. Concurrently, in future studies, we aim to measure the dimensions of the facet joint in advance for 3D printing, enabling the creation of a new FJFF device precisely tailored to the joint structure. Alternatively, multiple new FJFF devices could be pre-manufactured via 3D printing, allowing the most suitable device to be selected based on the joint structure during surgery.

5 | Conclusions

These findings suggest that the FJFF device is a viable alternative to traditional pedicle screw fixation, offering enhanced stability during lumbar fusion. It may provide a new option for the surgical treatment of patients with low back pain caused by FJOA in the future. Further verification through in vitro human specimens and in vivo animal experiments is required, along with necessary improvements to align the device more closely with human conditions, before advancing to clinical application research.

Author Contributions

Feilong Sun: conceptualization, methodology, writing – original draft, writing – review and editing, software. **Haiyang Qiu:** investigation, data curation. **Yufei Ji:** data curation, formal analysis. **Longchao Wang:** software, resources. **Wei Lei:** supervision, methodology. **Yang Zhang:** formal analysis, writing – review and editing, funding acquisition, project administration. All authors read and approved the final manuscript.

Acknowledgments

We thank the Key Laboratory of Orthopedics, Xijing Hospital Affiliated to the Air Force Medical University. This work was supported by the Key R&D Program of Shaanxi Province of China (2023-YBSF-146).

Conflicts of Interest

The authors declare no conflicts of interest.

References

1. A. C. Gellhorn, J. N. Katz, and P. Suri, "Osteoarthritis of the Spine: The Facet Joints," *Nature Reviews Rheumatology* 9, no. 4 (2013): 216–224.

2. L. T and D. AM, "Spinal Osteoarthritis," in *StatPearls* (StatPearls Publishing, 2023).

3. B. Meng, J. Bunch, D. Burton, and J. Wang, "Lumbar Interbody Fusion: Recent Advances in Surgical Techniques and Bone Healing Strategies," *European Spine Journal* 30, no. 1 (2021): 22–33.

4. A. Y. Aleinik, S. G. Mlyavykh, and S. Qureshi, "Lumbar Spinal Fusion Using Lateral Oblique (Pre-Psoas) Approach (Review)," *Sovremennye Tehnologii v Medicine* 13, no. 5 (2021): 70–81.

5. G. Fang, Y. Lin, J. Wu, et al., "Biomechanical Comparison of Stand-Alone and Bilateral Pedicle Screw Fixation for Oblique Lumbar Interbody Fusion Surgery—A Finite Element Analysis," *World Neurosurgery* 141 (2020): e204–e212.

6. X. Zhang, Y. Wang, W. Zhang, et al., "Perioperative Clinical Features and Long-Term Prognosis After Oblique Lateral Interbody Fusion (OLIF), OLIF With Anterolateral Screw Fixation, or OLIF With Percutaneous Pedicle Fixation: A Comprehensive Treatment Strategy for Patients With Lumbar Degenerative Disease," *Neurospine* 20, no. 2 (2023): 536–549.

7. L. Simon, F. Millot, X. Hoarau, R. Buttin, and R. Srour, "Comparison of the Biomechanical Effect of the FFX Device Compared With Other Lumbar Fusion Devices: A Finite Element Study," *International Journal of Spine Surgery* 16, no. 5 (2022): 935–943.

8. A. Welch-Phillips, D. Gibbons, D. P. Ahern, and J. S. Butler, "What Is Finite Element Analysis?," *Clinical Spine Surgery* 33, no. 8 (2020): 323–324.

9. Z. X. Liu, Z. W. Gao, C. Chen, et al., "Effects of Osteoporosis on the Biomechanics of Various Supplemental Fixations Co-Applied With Oblique Lumbar Interbody Fusion (OLIF): A Finite Element Analysis," *BioMed Central Musculoskeletal Disorders* 23, no. 1 (2022): 794.

10. X. Y. Cai, H. M. Bian, C. Chen, X. L. Ma, and Q. Yang, "Biomechanical Study of Oblique Lumbar Interbody Fusion (OLIF) Augmented With Different Types of Instrumentation: A Finite Element Analysis," *Journal of Orthopaedic Surgery and Research* 17, no. 1 (2022): 269.

11. X. Y. Cai, M. S. Sun, Y. P. Huang, et al., "Biomechanical Effect of L_4-L_5 Intervertebral Disc Degeneration on the Lower Lumbar Spine: A Finite Element Study," *Orthopaedic Surgery* 12, no. 3 (2020): 917–930.

12. W. Fan and L. X. Guo, "Influence of Different Frequencies of Axial Cyclic Loading on Time-Domain Vibration Response of the Lumbar Spine: A Finite Element Study," *Computers in Biology and Medicine* 86 (2017): 75–81.

13. H. W. Choi and Y. E. Kim, "Effect of Lumbar Fasciae on the Stability of the Lower Lumbar Spine," *Computer Methods in Biomechanics and Biomedical Engineering* 20, no. 13 (2017): 1431–1437.

14. G. R. Srinivas, M. N. Kumar, and A. Deb, "Adjacent Disc Stress Following Floating Lumbar Spine Fusion: A Finite Element Study," *Asian Spine Journal* 11, no. 4 (2017): 538–547.

15. L. Kalichman, L. Li, D. H. Kim, et al., "Facet Joint Osteoarthritis and Low Back Pain in the Community-Based Population," *Spine* 33, no. 23 (2008): 2560–2565.

16. M. Dreischarf, T. Zander, A. Shirazi-Adl, et al., "Comparison of Eight Published Static Finite Element Models of the Intact Lumbar Spine: Predictive Power of Models Improves When Combined Together," *Journal of Biomechanics* 47, no. 8 (2014): 1757–1766.

17. A. Rohlmann, T. Zander, M. Rao, and G. Bergmann, "Realistic Loading Conditions for Upper Body Bending," *Journal of Biomechanics* 42, no. 7 (2009): 884–890.

18. M. Yang, G. Sun, S. Guo, et al., "The Biomechanical Study of Extraforaminal Lumbar Interbody Fusion: A Three-Dimensional Finite-Element Analysis," *Journal of Healthcare Engineering* 2017 (2017): 9365068.

19. S. Vadapalli, K. Sairyo, V. K. Goel, et al., "Biomechanical Rationale for Using Polyetheretherketone (PEEK) Spacers for Lumbar Interbody Fusion-A Finite Element Study," *Spine* 31, no. 26 (2006): E992–E998.

20. C. C. Pan, C. H. Lee, K. H. Chen, Y. C. Yen, and K. C. Su, "Comparative Biomechanical Analysis of Unilateral, Bilateral, and Lateral Pedicle Screw Implantation in Oblique Lumbar Interbody Fusion: A Finite Element Study," *Bioengineering (Basel)* 10, no. 11 (2023): 1238.

21. R. K. Eastlack, P. D. Nunley, K. A. Poelstra, et al., "Finite Element Analysis Comparing a PEEK Posterior Fixation Device Versus Pedicle Screws for Lumbar Fusion," *Journal of Orthopaedic Surgery and Research* 18, no. 1 (2023): 855.

22. M. Song, K. Sun, Z. Li, et al., "Stress Distribution of Different Lumbar Posterior Pedicle Screw Insertion Techniques: A Combination Study of Finite Element Analysis and Biomechanical Test," *Scientific Reports* 11, no. 1 (2021): 12968.

23. A. Goel, A. Shah, M. Jadhav, and S. Nama, "Distraction of Facets With Intraarticular Spacers as Treatment for Lumbar Canal Stenosis: Report on a Preliminary Experience With 21 Cases," *Journal of Neurosurgery. Spine* 19, no. 6 (2013): 672–677.

24. A. Goel, "Facet Distraction Spacers for Treatment of Degenerative Disease of the Spine: Rationale and an Alternative Hypothesis of Spinal Degeneration," *Journal of Craniovertebral Junction and Spine* 1, no. 2 (2010): 65–66.

25. S. R. Satoskar, A. A. Goel, P. H. Mehta, and A. Goel, "Quantitative Morphometric Analysis of the Lumbar Vertebral Facets and Evaluation of Feasibility of Lumbar Spinal Nerve Root and Spinal Canal Decompression Using the Goel Intraarticular Facetal Spacer Distraction Technique: A Lumbar/Cervical Facet Comparison," *Journal of Craniovertebral Junction and Spine* 5, no. 4 (2014): 157–162.

26. R. Srour, Y. Gdoura, M. Delaitre, et al., "Facet Arthrodesis With the FFX Device: One-Year Results From a Prospective Multicenter Study," *International Journal of Spine Surgery* 14, no. 6 (2020): 996–1002.

27. R. Srour, "Comparison of Operative Time and Blood Loss With the FFX® Device Versus Pedicle Screw Fixation During Surgery for Lumbar Spinal Stenosis: A Retrospective Cohort Study," *Cureus* 14, no. 3 (2022): e22931.

28. F. Zairi, T. P. Sunna, H. J. Westwick, et al., "Mini-Open Oblique Lumbar Interbody Fusion (OLIF) Approach for Multi-Level Discectomy and Fusion Involving L5-S1: Preliminary Experience," *Orthopaedics & Traumatology, Surgery & Research* 103, no. 2 (2017): 295–299.

29. C. Silvestre, J. M. Mac-Thiong, R. Hilmi, and P. Roussouly, "Complications and Morbidities of Mini-Open Anterior Retroperitoneal Lumbar Interbody Fusion: Oblique Lumbar Interbody Fusion in 179 Patients," *Asian Spine Journal* 6, no. 2 (2012): 89–97.

30. H. M. Mayer, "A New Microsurgical Technique for Minimally Invasive Anterior Lumbar Interbody Fusion," *Spine* 22, no. 6 (1997): 691–700.

31. D. Sun, W. Liang, Y. Hai, P. Yin, B. Han, and J. Yang, "OLIF Versus ALIF: Which Is the Better Surgical Approach for Degenerative Lumbar Disease? A Systematic Review," *European Spine Journal* 32, no. 2 (2023): 689–699.

32. W. He, D. He, Y. Sun, et al., "Standalone Oblique Lateral Interbody Fusion vs. Combined With Percutaneous Pedicle Screw in Spondylolisthesis," *BioMed Central Musculoskeletal Disorders* 21, no. 1 (2020): 184.

33. S. S. Virk, S. Niedermeier, E. Yu, and S. N. Khan, "Adjacent Segment Disease," *Orthopedics* 37, no. 8 (2014): 547–555.

34. K. Hashimoto, T. Aizawa, H. Kanno, and E. Itoi, "Adjacent Segment Degeneration After Fusion Spinal Surgery—A Systematic Review," *International Orthopaedics* 43, no. 4 (2019): 987–993.

35. T. Lund and T. R. Oxland, "Adjacent Level Disk Disease—Is It Really a Fusion Disease?," *Orthopedic Clinics of North America* 42, no. 4 (2011): 529-viii.

36. C. S. Lee, C. J. Hwang, S. W. Lee, et al., "Risk Factors for Adjacent Segment Disease After Lumbar Fusion," *European Spine Journal* 18, no. 11 (2009): 1637–1643.

37. S. L. Weinhoffer, R. D. Guyer, M. Herbert, and S. L. Griffith, "Intradiscal Pressure Measurements Above an Instrumented Fusion. A Cadaveric Study," *Spine* 20, no. 5 (1995): 526–531.

38. B. W. Cunningham, Y. Kotani, P. S. McNulty, A. Cappuccino, and P. C. McAfee, "The Effect of Spinal Destabilization and Instrumentation on Lumbar Intradiscal Pressure: An In Vitro Biomechanical Analysis," *Spine* 22, no. 22 (1997): 2655–2663.

39. M. Rana, J. K. Biswas, S. Roy, et al., "Measurement of Strain in the Rod for Lumbar Pedicle Screw Fixation: An Experimental and Finite Element Study," *Biomedical Physics & Engineering Express* 6, no. 6 (2020): 065035, https://doi.org/10.1088/2057-1976/abc607.

40. M. Rana, S. Roy, P. Biswas, S. K. Biswas, and J. K. Biswas, "Design and Development of a Novel Expanding Flexible Rod Device (FRD) for Stability in the Lumbar Spine: A Finite-Element Study," *International Journal of Artificial Organs* 43, no. 12 (2020): 803–810.

41. H. Kim, D. H. Lim, H. J. Oh, K. Y. Lee, and S. J. Lee, "Effects of Nonlinearity in the Materials Used for the Semi-Rigid Pedicle Screw Systems on Biomechanical Behaviors of the Lumbar Spine After Surgery," *Biomedical Materials* 6, no. 5 (2011): 055005.